Soil Structure and Mixing Controls on WaterRock Contact: Implications for Enhanced Weathering

Water Resources Research

RESEARCH ARTICLE
10.1029/2025WR041479

Special Collection:
Quantifying Nature-based Climate Solutions

Soil Structure and Mixing Controls on Water-Rock Contact: Implications for Enhanced Weathering

Shashank Kumar Anand[1], **Matteo Bertagni**[2], **Felipe Aburto**[3], **and Salvatore Calabrese**[1]

[1]Department of Biological and Agricultural Engineering, Texas A&M University, College Station, TX, USA, [2]Department of Environment, Land and Infrastructure Engineering, Turin, Italy, [3]Department of Soil and Crop Sciences, Texas A&M University, College Station, TX, USA

Key Points:

- We developed a soil-physics-based framework to quantify the wet surface area (SA) of rock powder (RP) particles in heterogeneous, multiphase soils
- Wet SA varies by orders of magnitude with changes in soil structure, moisture, and the degree of RP mixing
- The framework can explain part of the theory-observation mismatch in enhanced weathering applications

Supporting Information:

Supporting Information may be found in the online version of this article.

Correspondence to:

S. K. Anand,
skanand@tamu.edu

Citation:

Anand, S. K., Bertagni, M., Aburto, F., & Calabrese, S. (2026). Soil structure and mixing controls on water-rock contact: Implications for Enhanced weathering. *Water Resources Research*, *62*, e2025WR041479. https://doi.org/10.1029/2025WR041479

Received 27 JUN 2025
Accepted 16 JAN 2026

Author Contributions:

Conceptualization: Shashank Kumar Anand, Salvatore Calabrese
Funding acquisition: Salvatore Calabrese
Investigation: Shashank Kumar Anand
Methodology: Shashank Kumar Anand
Project administration: Salvatore Calabrese
Software: Shashank Kumar Anand, Matteo Bertagni
Supervision: Salvatore Calabrese
Validation: Shashank Kumar Anand
Visualization: Shashank Kumar Anand

Abstract Enhanced weathering (EW), the addition of finely ground silicate rock powder (RP) to soil, has emerged as a promising carbon removal strategy. However, quantifying weathering rates in soils remains challenging, as most continuum-scale EW models do not adequately account for the fraction of RP surface area (SA) that is wet at a given soil moisture and thus actively weathering. Here, we study how soil pore structure, RP particle size distribution, and RP mixing degree within the soil control water-rock contact. Using a soil-physics-based framework, we derive a scaling factor that quantifies the wet fraction of RP SA as a function of soil moisture and mixing degree within soil pores. This scaling factor varies nonlinearly with soil moisture for typical soil pore structures and RP particle size distributions, countering previous zero-order (independent of soil moisture) or linear assumptions. The scaling factor evolves dynamically with hydrological fluctuations and, for a given pore structure and RP mixing degree, it can span nearly two orders of magnitude with changes in median particle size. To illustrate its application, we integrate the derived scaling factor into the Soil Model for Enhanced Weathering and examine the sensitivity of simulated weathering fluxes to mixing degree under otherwise identical conditions. Under low mixing, results show that average weathering rates are roughly two orders of magnitude lower than under perfect mixing over 1 year of application. Our work provides a mechanistic, computationally efficient framework for representing water-rock contact in soil, offering a pathway to improve continuum-scale EW models.

Plain Language Summary Enhanced weathering (EW) is a strategy that spreads finely ground silicate rock powder (RP) over soils to remove atmospheric carbon dioxide (CO_2). However, predicting how fast the RP weathers and therefore how much CO_2 it can remove remains highly uncertain in soils. This is partly because most continuum-scale EW models assume that the entire surface area (SA) of the added RP is always in contact with water. Here, we show that the degree of RP mixing in the soil, the soil pore structure, and the level of soil moisture all strongly influence the portion of the rock surface that is actually in contact with water and can react. We develop a new, soil-physics-based framework to calculate the "wet" fraction of the RP SA under different soil and mixing conditions. We find that this wet fraction varies nonlinearly with soil moisture levels and the degree of mixing, which in turn affects the overall weathering rate of the added rock particles. Our framework helps explain part of why observed weathering rates in the field are often lower than predicted. It also provides a practical way to improve continuum-scale EW models and better estimate the carbon removal potential of EW.

1. Introduction

Enhanced weathering (EW), which consists of amending agricultural or forest soils with pulverized silicate rocks, is a promising Carbon Dioxide Removal (CDR) technology with significant potential to store carbon for geologic timescales and low technological barriers (Beerling et al., 2025; Hartmann et al., 2013; Köhler et al., 2010). Yet, it remains one of the most unconstrained CDR technologies in terms of realized carbon removal rates due to both experimental quantification and modeling challenges (Buckingham et al., 2022; Calabrese et al., 2022; Clarkson et al., 2024; H. Deng et al., 2023; Power et al., 2025). With a growing interest in EW (Gaucher et al., 2025; Kantzas et al., 2022; Paulo et al., 2021) and the global CDR market (Michaelowa et al., 2023; Smith et al., 2024; Sovacool et al., 2023), it is critical to innovate on experimental and theoretical approaches that can accurately quantify and predict rates of CDR across diverse soil types, climates, and deployment characteristics.

Writing – original draft: Shashank Kumar Anand
Writing – review & editing: Matteo Bertagni, Felipe Aburto, Salvatore Calabrese

In soils, silicate RP particles (typically pulverized to silt size, 10–1,000 μm) interact with water and dissolved CO_2, leading to mineral dissolution, alkalinity release, and aqueous bicarbonate formation (Bertagni & Porporato, 2022; Hartmann et al., 2013). As these weathering products follow the hydrological cycle, they can precipitate on land, forming carbonate minerals (this reduces the CO_2 sequestration by half), they can be partially lost to soil absorption and plant uptake (Calabrese et al., 2022; Hartmann et al., 2013), or they can remain in the water and ultimately reach the ocean (Bertagni & Porporato, 2022; Zhang et al., 2025), mitigating ocean acidification (Renforth & Campbell, 2021; Taylor et al., 2016) and storing carbon for geological timescales (Archer et al., 1997; Renforth & Henderson, 2017). At the global scale, recent techno-economic studies set the CO_2 sequestration potential of EW on the order of Giga tonnes CO_2 yr^{-1} if broadly implemented by highly emitting countries (Beerling et al., 2020, 2025; Strefler et al., 2018). Realizing the potential of EW requires optimizing deployment, which hinges on improving predictions and quantifying the uncertainties of RP dissolution rates.

While CDR estimates for EW show promise, significant uncertainties persist, particularly concerning the initiation of CO_2 removal in soils, which is governed by RP dissolution rates (Andrews & Taylor, 2019; Brantley, 2025; White & Brantley, 2003). Even natural mineral weathering rates are highly variable (Brantley, 2025), strongly influenced by temperature (K. Deng et al., 2022), climate aridity (Calabrese & Porporato, 2020), and ecosystem properties (Hunt, 2021). Extrapolating laboratory findings, which are often obtained under controlled extrinsic parameters such as temperature and pH, tends to yield dissolution rates that deviate from those observed in the field, posing a well-known challenge in geokinetics (Pačes, 1983; White & Blum, 1995; Brantley, 2025). Most weathering rate estimations to date have been conducted in agitated, abiotic acid-filled flasks (Palandri and Kharaka, 2004), which limits our understanding of how added RP behaves in the complex, multiphase soil environments encountered in EW applications (Calabrese et al., 2022; H. Deng et al., 2023; Klemme et al., 2022; Power et al., 2025; White & Brantley, 2018). This added layer of complexity makes the uncertainty in RP dissolution rates particularly dominant in EW applications, as emphasized in a recent model-experiment comparison (Bertagni et al., 2025).

From a mechanistic standpoint, the structure of the soil pore space and the spatial distribution of added RP particles within it exerts a critical control over the fraction of RP surface area (SA) that comes into contact with water at any given time. Although pore-scale reactive transport modeling has made significant strides in quantifying water–rock powder collocation and improving estimates of weathering fluxes in soils (Jung & Navarre-Sitchler, 2018; L. Li et al., 2006; Molins et al., 2012; Parmigiani et al., 2011), such models remain computationally intensive and can be challenging to scale for modeling large-scale EW predictions. Meanwhile, continuum-scale models used to estimate EW potential at field or regional scales typically do not incorporate pore-scale information about soil structure, RP particle characteristics, or the degree of mixing, all of which directly influence the wet fraction of the SA of the added RP that can react.

In continuum-scale reactive transport (Beerling et al., 2020; K. Deng et al., 2022; Kanzaki et al., 2022; Kanzaki et al., 2024; Taylor et al., 2016) and ecohydrological (Bertagni et al., 2025; Cipolla et al., 2021a, 2021b) models for EW, weathering fluxes are generally calculated as the product of the weathering rate per unit SA (W_r, in mol m^{-2} s^{-1}), typically derived from standard kinetic formulations dependent on pH and temperature (Palandri and Kharaka, 2004), and the total SA of applied RP. The latter is estimated either through direct measurement or inferred from particle size distributions. One-dimensional reactive transport models often assume that the entire rock surface is always actively reacting, effectively treating all added RP as continuously exposed to soil water (Beerling et al., 2020; Kanzaki et al., 2022), while zero-dimensional ecohydrological and biogeochemical models tend to scale wet SA linearly with soil moisture level (Bertagni et al., 2025; Cipolla et al., 2021b). Neither approach considers how the spatial distribution of water and RP particles within the soil matrix, a function of soil structure, RP particle size distribution, and mixing, influences the dynamics of the wetted SA.

Motivated by the lack of parameterizations for interactions among soil structure, RP particles, and water, we develop a soil-physics-based scaling framework at the continuum scale to estimate the fraction of RP SA that is wet and therefore actively contributing to weathering at a given time. Our theoretical approach explicitly incorporates small-scale information on soil structure, RP particle characteristics, and degree of mixing. In Section 2, we present the theoretical basis for our approach, deriving a scaling factor for the wet SA and introducing a parsimonious metric to quantify rock-particle mixing within soil pores. In Section 3, we explore the influence of soil texture and a range of RP sizes on the scaling of the wet SA with soil saturation. To demonstrate the applicability of our framework, we then incorporate the dynamic scaling factor into the Soil Model for Enhanced

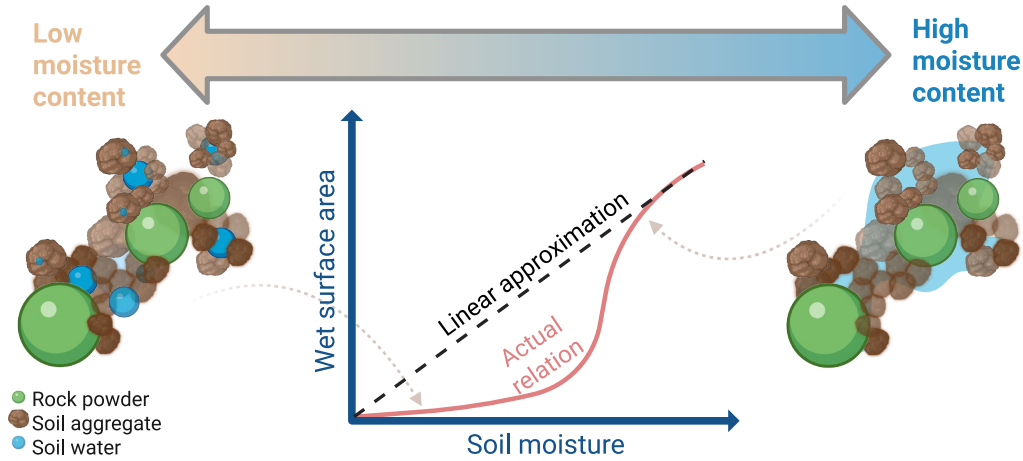

Figure 1. Soil pore structure controls the extent of water contact with added rock powder (RP) particles at a given degree of soil moisture saturation. In enhanced weathering applications, a common assumption is a zero-order response with full wetting ($\xi = 1$) (Beerling et al., 2020; Kanzaki et al., 2022; Taylor et al., 2016), or a linear relationship with saturation, $\xi = s$ (Bertagni et al., 2025; Sverdrup & Warfvinge, 1988). We expand upon these empirical approximations by accounting for the spatial overlap between water-filled pores and the positions of RP particles within the soil pore structure, obtaining a nonlinear dependence of ξ on soil moisture.

Weathering (SMEW) (Bertagni et al., 2025) to quantify the impact of our novel expression for the wet SA on EW applications under varying hydrological conditions and rock-particle mixing scenarios. This application is intended only to investigate the sensitivity of RP dissolution to the scaling factor, rather than to estimate actual weathering rates. Finally, Section 4 concludes with implications of the proposed framework for improving estimates of reactive RP SA in continuum-scale EW models and discusses future directions for modeling improvements and experimental validation.

2. Linking Water Contact of Rock Powder to Soil Structure at the Continuum Scale

As RP particles are added to soils, their wet SA (SA_{wet}) at any time (t) depends on their contact with soil water and, thus, will be only a portion of the total SA. This relationship can be expressed as

$$SA_{wet}(t) = \xi(t)\, SA, \tag{1}$$

where ξ is a scaling factor for the wet SA, ranging from 0 to 1. Due to the lack of a mechanistic theoretical framework, most continuum-scale EW models to date either assumed $\xi = 1$ (Beerling et al., 2020; Kanzaki et al., 2022; Taylor et al., 2016), that is, all SA of the added RP is continuously in contact with soil water, or scaled it linearly with degree of saturation of soil pores (Bertagni et al., 2025; Cipolla et al., 2021b), as illustrated in Figure 1. We will show that ξ is a strongly nonlinear function of soil saturation that also depends on soil pore structure, RP particle size distribution, and the degree of RP mixing within the soil matrix.

2.1. Conceptualizing the Wet Surface Area as a Function of Soil Moisture

To mathematically formulate ξ, it is helpful to recall that the soil matrix comprises an arrangement of random-sized aggregates, with the pore space between them occupied by air and water (Dlapa et al., 2020; X. Li & Zhang, 2009; Nimmo, 2004). At equilibrium, water occupies the smallest pores with higher tension (more negative water potential) and fills progressively larger pores as soil water saturation increases. Following a common representation in soil physics and hydrology (Brutsaert, 2023; Porporato & Yin, 2022), we characterize the soil pore space ζ as a bundle of capillary tubes, with $\zeta_{p_{min}}$ and $\zeta_{p_{max}}$ denoting the smallest and largest pore tube sizes, respectively. At equilibrium, the soil pore size distribution $f_p(\zeta)$ and the relative soil moisture s (i.e., the degree of pore saturation) are then related by

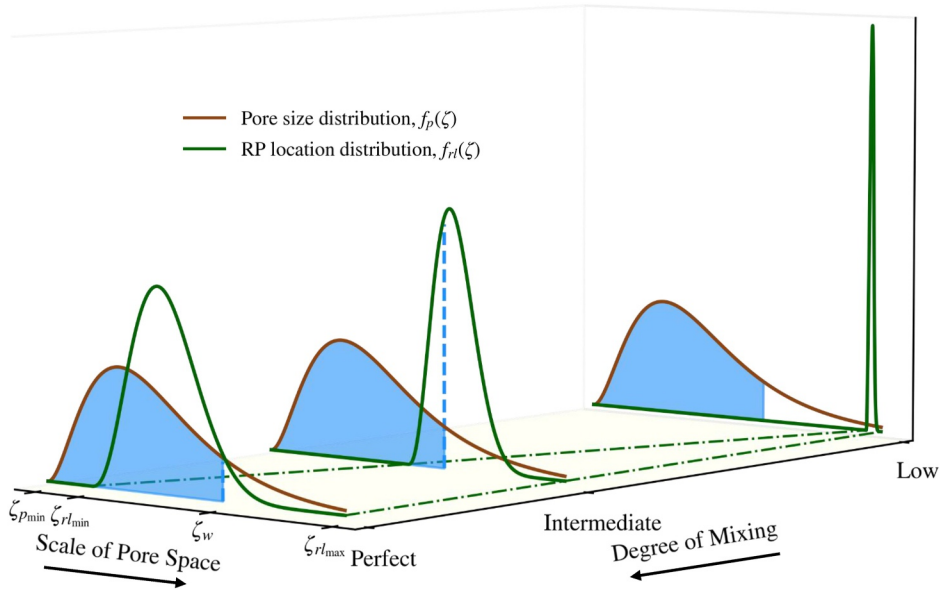

Figure 2. Influence of soil pore structure and degree of mixing on water availability for rock powder (RP) particles in the soil pore space ζ. The soil pore size distribution ($f_p(\zeta)$) is shown in brown, and the distribution of RP particle locations within the pore space ($f_{rl}(\zeta)$) is shown in green. The largest water-filled pore (ζ_w), indicated by dashed blue lines, indicates water availability for RP particle dissolution. The smallest pore accessible to RP particles depends on their size and the degree of mixing. Under low mixing, RP particles are confined to larger pores; as mixing increases, they can access smaller pores. Under perfect mixing, the location distribution matches the RP particle size distribution.

$$\int_{\zeta_{p_{\min}}}^{\zeta_w} f_p(\zeta)d\zeta = F_p(\zeta_w) = s \tag{2}$$

where ζ_w corresponds to the largest soil pore size occupied by soil water. In other words, the cumulative pore size distribution $F_p(\zeta_w)$ corresponds to the relative soil moisture s. This equals one when ζ_w reaches the largest pore size $\zeta_{p_{\max}}$ (all soil pores are water-filled) and tends to zero as soil dries and ζ_w approaches the smallest pore size $\zeta_{p_{\min}}$. This relationship is the standard soil physics approach linking pore size distribution to hydraulic properties, such as water retention and hydraulic conductivity at the continuum scale (Brutsaert, 2023; Hillel, 2013; Mualem, 1976; Van Genuchten, 1980), and here, and it provides the basis for determining the fraction of added RP SA that is in contact with water.

As water potential becomes more negative with decreasing soil moisture level, water becomes increasingly confined to smaller soil pores. Consequently, for RP particles in unsaturated soil ($s < 1$), the fraction of particles located in small, water-filled pores will be in contact with water and therefore reactive, whereas particles located in larger, air-filled pores will not. This behavior is illustrated schematically in Figure 1, where the fraction of wet reactive SA approaches 0 as the soil dries and approaches 1 as the soil becomes saturated (due to rainfall or irrigation). How the fraction of wet RP SA varies with soil moisture thus depends on the available pores and where the RP particles are located, that is, the overlap between soil pore and RP particle location distributions in the space of ζ.

The location of added RP particles within the soil pore space depends upon their sizes, as a particle of diameter d can only occupy a pore of size ζ equal to or larger than d, $\zeta \geq d$, as well as the degree to which they are mixed into the soil. Without significant mixing, RP particles of diameter d are likely to be deposited in larger pores, limiting their interaction with water. With a higher degree of RP mixing in soil, particles are more likely to reach pores close to their size $\approx d$, a fact that may increase their chances of interacting with water. As a result, for a given soil pore size distribution (brown curve in Figure 2), the distribution of added RP particle locations (hereafter, RP location distribution $f_{rl}(\zeta)$; green curve in Figure 2) is concentrated and peaked around the largest pores under low mixing. As the mixing increases, the RP location distribution more closely approximates the actual RP particle size distribution (subject to the constraint $\zeta \geq d$).

2.2. Quantifying the Surface Area Scaling Factor and the Degree of Mixing

We mathematically formulate the scaling factor for wet SA by considering RP diameters d ranging from a minimum $d_{\min}$ to a maximum $d_{\max}$, with a size distribution $f_{rd}(d)$. Within the soil pore space ζ, these particles occupy pores ranging from $\zeta_{rl_{\min}}$ to $\zeta_{rl_{\max}}$, described by a location distribution $f_{rl}(\zeta)$. Assuming the existence of a function, informed by experimental observations or theoretical considerations, that links rock diameters d to the pore size ζ where they are located, denoted as $d = \mathcal{M}(\zeta, \alpha)$, where α quantifies the degree of mixing (see below), a mathematical expression for the scaling factor ξ in Equation 1 can be derived. The general time-varying form of ξ depends on the mixing degree, soil moisture s, the soil pore size distribution $f_p(\zeta)$, and the RP location distribution $f_{rl}(\zeta)$, and is given by

$$\xi = \begin{cases} 0 & \zeta_w(s) \le \zeta_{rl_{\min}}, \\ \dfrac{\int_{\zeta_{rl_{\min}}}^{\zeta_w} \mathcal{M}(\zeta,\alpha)^2 \times f_{rl}(\zeta)d\zeta}{\int_{\zeta_{rl_{\min}}}^{\zeta_{rl_{\max}}} \mathcal{M}(\zeta,\alpha)^2 \times f_{rl}(\zeta)d\zeta} & \zeta_{rl_{\min}} < \zeta_w(s) < \zeta_{rl_{\max}}, \\ 1 & \zeta_{rl_{\max}} \le \zeta_w(s), \end{cases} \tag{3}$$

where ζ_w is related to soil moisture s based on Equation 2. As a result, any changes in the soil pore structure (for a known $f_p(\zeta)$ at a given time) can be readily incorporated into the calculation of ξ, including changes that arise from different mixing operations that significantly alter the soil pore distribution.

Equation 3 expresses the fact that the SA scaling factor ξ is given by the total (viz., the integral) SA of particles located in the smaller water-filled pores. ξ equals zero when soil moisture is low enough that only the smallest pores (smaller than the minimum pore occupied by the particles, i.e., $\zeta_{rl_{\min}}$) are filled with water. ξ approaches one under well-watered conditions, where the largest pores occupied by the particles are also filled with water ($\zeta_w \ge \zeta_{rl_{\max}}$). For intermediate conditions, ξ is determined by the normalized second moment of the RP location distribution, and the upper integration limit is given by $\zeta_w(s)$, which corresponds to the blue-colored region under the $f_p(\zeta)$ curve in Figure 2.

Given that, in EW experiments, it is challenging to measure the spatial distribution of RP particles within the soil matrix, we characterize the degree of mixing between RP particles and soil pores by defining α as the normalized linear distance between the particle size d and the pore size ζ (equal or larger than d) in which the RP particle is located,

$$\alpha = \frac{\zeta - d_{\max}}{d - d_{\max}}. \tag{4}$$

By inverting Equation 4 to obtain d, the function linking RP particle location to particle size can be expressed as $\mathcal{M}(\zeta, \alpha) = (\zeta - (1 - \alpha)\, d_{\max})/\alpha$. The underlying assumption in this characterization is that Equation 4 applies across all RP particle sizes. Although this relationship could be adjusted if more detailed information on RP particle-level mixing were available from experimental evidence or theoretical considerations, such information is generally not available in EW studies and lies outside the continuum scale typically used in EW modeling.

α approaches one in the case of perfect mixing, where all RP particles of size d occupy soil pores of size $\zeta = d$. In contrast, a decrease in the value of α indicates reduced mixing. For instance, when $\alpha = 0.5$, each RP particle is located, on average, in a pore midway between its own size and the maximum RP size. As a result, $\zeta_{rl_{\min}}$ shifts halfway toward $\zeta_{rl_{\max}}$, which, according to Equation 3, leads to $\xi = 0$ if the largest water-filled pore ζ_w does not exceed this shifted threshold. Consequently, a large fraction of the smaller particles is excluded from finer, water-filled pores closer to their own size, substantially reducing their potential contact with water compared to perfect mixing ($\alpha = 1$). A low value such as $\alpha = 0.5$, therefore, corresponds to a low mixing scenario, where even small RP particles are clustered in coarser pores, such as after surficial RP application that leaves particles initially residing in large pores near the soil surface. Even in such cases, however, the effective mixing degree can vary both vertically and temporally as particles are mixed by natural or anthropogenic processes within the soil substrate. This is further discussed in Section 4.

2.3. Analytical Expression for ξ Under Perfect Mixing

A commonly reported shape for RP particle size distribution is the one of a log-normal (Beerling et al., 2020; Hartmann et al., 2013), which can also be reproduced by a truncated gamma distribution. From a theoretical perspective, if $f_{rd}(d)$ is represented by a gamma distribution with shape parameter η and scale parameter θ, that is,

$$f_{rd}(d;\gamma,\theta) = \frac{1}{N_d} d^{\eta-1} e^{-d/\theta}, \tag{5}$$

where the normalization constant N_d is equal to $\Gamma(\eta) \times \theta^{\eta}$ as rock diameter d ranges from $d_{\min} \to 0$ to $d_{\max} \to \infty$ and $\Gamma(\cdot)$ denotes the gamma function (Abramowitz & Stegun, 1965).

Under the assumption of perfect mixing (i.e., $\alpha = 1$ and $\mathcal{M}(\zeta) = \zeta$), a condition that may be obtained with time, after an initial artificial rock-soil mixing, as rainfall and bio-turbation redistribute the added RP particles within the soil matrix, the variation of scaling factor ξ in Equation 3 can be written analytically as

$$\xi = \frac{\int_{\zeta_{rl_{\min}}}^{\zeta_w} \zeta^{\eta+1} e^{-\zeta/\theta} d\zeta}{\int_{\zeta_{rl_{\min}}}^{\zeta_{rl_{\max}}} \zeta^{\eta+1} e^{-\zeta/\theta} d\zeta} = \frac{\int_{\zeta_{rl_{\min}}}^{\zeta_w} \zeta^{\eta+1} e^{-\zeta/\theta} d\zeta}{N_\zeta} = F_{rl}\left(\zeta_w;\eta+2,\theta\right), \tag{6}$$

which is an integral of a gamma distribution with an updated shape parameter $\eta + 2$ and a new normalization constant N_ζ in the pore space ζ. In other words, the cumulative gamma distribution $F_{rl}\left(\zeta_w;\eta+2,\theta\right)$ corresponds to the ξ at the relative soil moisture s. In the case of the integration limits $\zeta_{rl_{\min}} \to 0$ and $\zeta_{rl_{\max}} \to \infty$, ξ can be written explicitly as $\xi = \frac{1}{\Gamma(\eta+2)}\gamma\left(\eta+2, \frac{\zeta}{\theta}\right)$, where $\gamma(\cdot,\cdot)$ is the lower incomplete gamma function (Abramowitz & Stegun, 1965).

3. Results

To demonstrate the application of the framework derived in Section 2, we use Equations 3 and 4 to quantify how the SA scaling factor ξ, defined as the fraction of the total RP SA that is wet, varies with soil moisture across representative scenarios of RP particle sizes, soil pore size distributions, and the degree of mixing.

3.1. Nonlinear Dependence of the Wet Surface Area on Soil Moisture: Role of Pore Structure and Mixing

We adopt the double-exponential (DE) model (Dexter et al., 2008) to represent the soil pore structure here, which distinguishes between textural and structural pore domains and has been calibrated across various soil texture classes (Ding et al., 2016). While the DE model is employed here for the analysis, our theoretical framework for the wet SA is flexible and can be applied with other soil pore models, such as Brooks and Corey (Brooks, 1965), van Genuchten (Van Genuchten, 1980), and others (Hill et al., 1985; X. Li & Zhang, 2009), as well as with experimental pore size data (Nimmo, 2004; Wildenschild & Sheppard, 2013). In this analysis, we consider silt and loamy soils using the DE model parameters from Table 3 of Ding et al. (2016). Reported RP sizes in EW applications span a wide range from tens to thousands of micrometers (Amann et al., 2020; Kelland et al., 2020; te Pas et al., 2023). The RP particle size distribution is modeled here using a truncated gamma distribution with median diameters ranging from 50 to 450 μm, and a maximum cutoff of 1,000 μm to reflect practical limits of RP fragmentation.

To incorporate the effect of mixing on the wet SA, we apply Equation 4 to simulate low ($\alpha = 0.5$), intermediate ($\alpha = 0.75$), and perfect ($\alpha = 1$) mixing scenarios for each soil texture and rock size distribution. Computing the scaling factor using Equation 3 requires specifying a soil pore size distribution $f_p(\zeta)$ for each scenario. If $f_p(\zeta)$ can be directly estimated from the mixed (RP and soil) particle size distributions (as shown in Figures S1 and S2 in Supporting Information S1), that distribution can be used. Alternatively, $f_p(\zeta)$ can be approximated as the original soil pore size distribution, given that in standard conditions the mass (or volume) ratio between RP and soil substrate is low. This formulation allows us to isolate the sensitivity of the wet SA at a given soil moisture level to RP particle size and mixing degree, under otherwise similar soil pore structures.

10.1029/2025WR041479

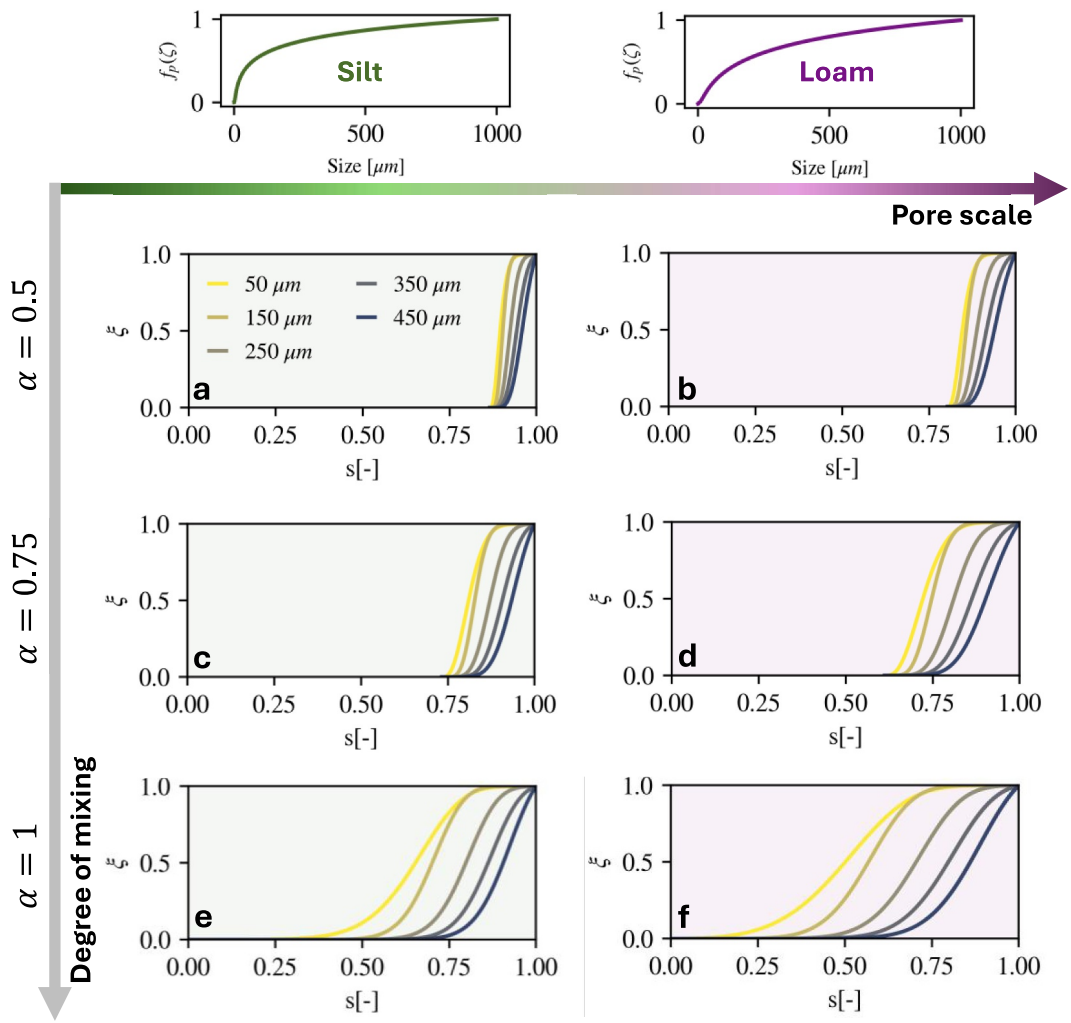

Figure 3. Scaling factor ξ for the wet surface area (SA), computed using Equation 3, shown as a function of relative soil moisture s under six different combinations of RP mixing and soil pore structure. Rows correspond to increasing degrees of mixing: low ($\alpha = 0.5$, top), intermediate ($\alpha = 0.75$, middle), and perfect mixing ($\alpha = 1$, bottom). Columns represent increasing soil coarseness, from silty-textured soil with finer pores (left) to loamy soil with coarser pores (right), based on the double-exponential model (Dexter et al., 2008). Each panel (a–f) displays $\xi(s)$ curves for particle size distributions with median diameters ranging from 50 μm (yellow) to 450 μm (blue). The combined effects of soil pore structure and mixing efficiency modulate the wet SA of the added particles nonlinearly with changing soil moisture.

The combination of soil textures and mixing degrees yields six distinct scenarios, each analyzed across various median RP sizes. Figure 3 presents the variation of the SA scaling factor ξ as a function of soil moisture across these scenarios, where soil texture increases from left to right, and mixing efficiency increases from top to bottom. Across all cases, we observe that ξ exhibits a highly nonlinear response with respect to soil moisture, clearly departing from the first-order linear approximation commonly used in past models (Bertagni et al., 2025; Cipolla et al., 2021b; Sverdrup & Warfvinge, 1988) or the zero-order responses implied in others (Beerling et al., 2020; Kantzas et al., 2022).

Figure 3 demonstrates that ξ becomes negligible at low soil moisture levels, as the RP does not come into contact with water-filled pores. The threshold soil moisture at which water-rock contact begins is influenced by the size of the RP particles and, even more, by the degree of mixing. Under perfect mixing, smaller particles access water-filled pores more readily, leading to higher ξ values even at lower moisture levels. For a given RP particle size distribution, an increase in soil pore size elevates ξ under drier conditions (e.g., Figures 3e and 3f), while reduced mixing suppresses it. For instance, in the intermediate mixing scenario (Figure 3d), ξ remains zero below 60% saturation ($s < 0.6$) because smaller particles fail to occupy the smallest available pores. In contrast, perfect

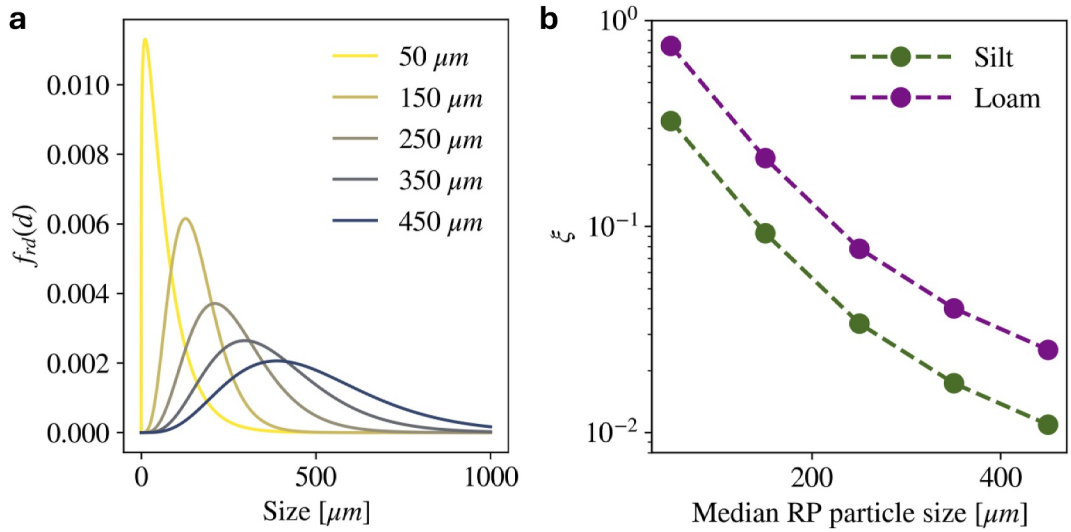

Figure 4. Variation of the SA scaling factor ξ with particle size under well-watered conditions. (a) Rock powder particle size distributions ($f_{rd}(d)$), with median sizes ranging from approximately 50 to 450 μm. (b) ξ in well-watered ($s = 0.6$) and perfect mixing ($\alpha = 1$) conditions, showing orders of magnitude variations as a function of the median RP particle size.

mixing in a loamy soil (Figure 3f) results in nonzero ξ values across a large range of soil moisture values well below 0.6.

3.2. Variation of the Surface Area Scaling Factor With Median Rock Size

Figure 4 presents the variability in the SA scaling factor ξ as a function of the median RP size. The analysis uses particle size distributions with median values ranging from 50 to 450 μm (Figure 4a) and evaluates the corresponding changes in ξ across two soil textures (loam and silt) under the assumption of perfect mixing. To isolate the influence of particle size on SA scaling under well-watered conditions, we compare ξ values at $s = 0.6$, representative of well-watered states for these soils (Laio et al., 2001; Porporato & Yin, 2022).

Even under favorable moisture conditions and ideal mixing, ξ spans nearly two orders of magnitude, indicating a strong sensitivity to particle size. This pronounced decline in ξ with increasing median particle size results from a growing mismatch between the larger dry pores occupied by coarser particles and the relatively smaller water-filled pores, which limits water-rock interaction even under perfect mixing. While Figure 4b focuses on median particle size, it is important to note that as mixing decreases (i.e., lower α), for fixed pore structure and particle size distribution the $\xi - s$ relation shifts further to the right (e.g., Figures 3a, 3c, and 3e), indicating lower ξ values at a given soil moisture. This highlights that while reducing particle size improves reactivity, the degree of mixing, and its evolution over time, can exert an equally strong control on effective wet SA, with implications for observed EW rates in soil. The next section explores this effect in detail using EW model simulations.

3.3. Implications for Enhanced Weathering Rates

To evaluate the implications of the derived scaling factor ξ on EW fluxes, we incorporated the ξ framework into the SMEW (Bertagni et al., 2025), an updated version of the original model developed by Cipolla et al. (2021b). SMEW is an ecohydrological and biogeochemical model designed to simulate weathering fluxes in the upper soil layers where RP particles are applied. SMEW has successfully reproduced several experimental observations, relying on an empirical, data-driven correction factor for the kinetic coefficients to match observed weathering rates. In most experimental cases, this factor is consistently less than one, pointing to uncertainties in kinetic coefficients likely originating from unaccounted processes affecting dissolution. While various abiotic and biotic controls may contribute to this uncertainty, the integration of the ξ scaling factor allows us to assess whether soil structure and RP particle sizes, via their influence on water-rock interaction, may partially explain the order of magnitude reduction in observed rates.

We developed and integrated a new weathering solver in SMEW based on Equation 3 and conducted a 1-year simulation of the application of 1 kg/m^2 of forsterite (Mg_2SiO_4) with a median grain size of 150 μm in a temperate humid climate and 30 cm loamy soil, evaluating distinct soil-water-rock interaction scenarios. The first model scenario, termed the zero-order approximation, assumes the entire RP SA is always wet ($\xi = 1$ in Equation 1). The second corresponds to the default configuration in the SMEW, where $SA_{wet}(t)$ is linearly scaled with the relative soil moisture ($\xi = s$). In the third scenario, ξ is computed based on soil texture, RP particle size distribution, and degree of mixing following Equation 3. In particular, we consider the case of perfect mixing ($\alpha = 1$), intermediate mixing ($\alpha = 0.75$), and low mixing ($\alpha = 0.5$). While the degree of mixing may evolve as particles dissolve and shrink, we assume a fixed α value over the simulation period, which is an optimistic scenario in which particles redistribute into smaller pores as they weather. All scenarios share identical environmental and soil parameters, including a mean annual temperature of 13°C and mean annual precipitation of 1,000 mm. The soil is an acidic loam (initial pH = 4) with an initial OC content of 5%, with a pore size distribution defined by the DE model (Figure 3). We evaluated that applying 1 kg m^{-2} of forsterite in 30 cm loamy soil produces only a 0.25% reduction in bulk soil porosity and negligible changes in the pore size distribution $f_p(\zeta)$ across mixing scenarios (Figure S1 in Supporting Information S1). Even when considering a shallower soil profile (20 cm) and a fivefold higher RP application rate, changes in bulk porosity and the pore size distribution remain small (Figure S2 in Supporting Information S1). Accordingly, we employ the same pore size distribution to compute ξ using Equation 3 for all RP mixing scenarios. This assumption can be relaxed for RP applications or mixing conditions under which RP addition or soil-disturbance processes substantially modify the pore structure.

Figure 5 presents the temporal evolution of the weathering flux and RP dissolution across the five scenarios for a numerically generated rainfall and soil moisture time series. The scenarios yield distinct temporal dynamics in dissolution rates, with the zero-order approximation yielding the highest total EW flux and the low-to-intermediate mixing cases exhibiting the lowest rates throughout the year (Figure 5b). The linear and perfect mixing scenarios fall between these two extremes. The zero-order approximation exhibits dynamics that is not directly linked to soil moisture, and is governed solely by soil biogeochemical conditions. The linear approximation, with slightly lower weathering rates, is moderately more variable, reflecting the influence of the soil moisture dynamics. All weathering rates estimated through mixing of pore size and particle size distributions are significantly more variable due to highly nonlinear dependence on soil moisture. This variability is greater for low mixing degrees, as high weathering rates arise only at high soil moisture when water eventually fills the larger pores where RP particles reside.

This sensitivity to the degree of RP mixing within the soil matrix influences the average total weathering rates across different mixing scenarios. Although the average rates under perfect mixing and a linear approximation are similar, the intermediate-to-perfect mixing scenario yields a weathering rate ratio of $\langle EW_{oliv,\alpha=0.75}\rangle / \langle EW_{oliv,\alpha=1}\rangle = 0.35$, while the low-to-perfect mixing ratio $\langle EW_{oliv,\alpha=0.5}\rangle / \langle EW_{oliv,\alpha=1}\rangle$ drops sharply to just 0.032. These high variations in EW rates highlight the strong control that mixing exerts on realized dissolution rates for a given soil type and initial rock distributions. Compared against the zero-order assumption, where the entire rock surface is assumed to be always wet, the average total weathering rate ratios are $\langle EW_{oliv,\alpha=1}\rangle / \langle EW_{oliv,zero}\rangle = 0.86$, $\langle EW_{oliv,\alpha=0.75}\rangle / \langle EW_{oliv,zero}\rangle = 0.3$, and $\langle EW_{oliv,\alpha=0.5}\rangle / \langle EW_{oliv,zero}\rangle = 0.03$. The implications of these rate differences become clearer in Figure 5c, which shows the evolution of residual rock mass under each scenario: low mixing leaves nearly 98% of the initial mass intact, whereas intermediate to perfect mixing reduces it to 78% and 37%, respectively. In comparison, the linear and zero-order cases show more extensive dissolution, with only 36% and 26% of the rock mass remaining.

Differences in weathering rate dynamics also affect the temporal evolution of RP particle size (Figure 6a) and, in turn, the scaling factor ξ. The zero-order scenario shows the most pronounced RP dissolution, whereas in the low mixing scenario, the distribution does not shift significantly over the year. All other scenarios fall in between. As particle sizes decrease, the scaling factor ξ, which depends on the particle size distribution, changes. In particular, the relationship between the proposed nonlinear scaling factor ξ and relative soil moisture s shifts leftward over time, reflecting the migration of dissolving RP particles into smaller soil pores. The importance of these temporal changes in ξ is evident when comparing with typical approximations. For example, consider the perfect mixing and linear approximation scenarios, for which the average dissolution rates are comparable. Due to the shape of ξ (Figure 6b), the linear approximation overestimates ξ at low soil moisture saturation and underestimates it at high

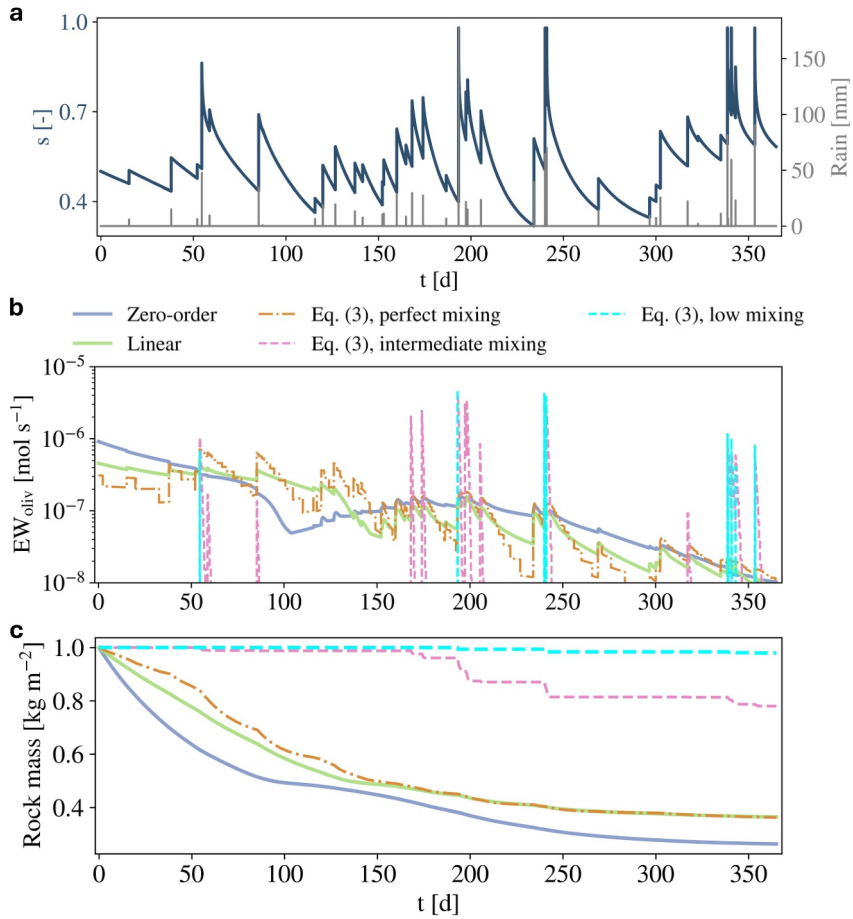

Figure 5. Impact of the ξ scaling factor on the simulated weathering rates. Simulation run with Soil Model for Enhanced Weathering (SMEW) for an application of forsterite (1 kg m^{-2}) in 30 cm loamy soil (pore structure following Figure 3) of a temperate humid climate (mean annual rainfall = 1,000 mm, mean annual temperature = 13°C). (a) Rainfall and soil moisture time series. (b) Enhanced weathering rates under different approximation: for the proposed soil structure approach, the cases of low ($\alpha = 0.5$), intermediate ($\alpha = 0.75$), and perfect mixing ($\alpha = 1$) are considered and compared to the baseline cases with zero ($SA_{wet}(t)$ equal to $SA(t)$ in Equation 1 for all time t) or first order (linear dependence of wet surface area on the relative soil moisture, i.e., $\xi(t) = s(t)$ as the default case of SMEW). (c) Temporal dynamics of mineral rock powder mass over the year, with the percentage of rock mass remaining at the end of the year being 98%–37% in low to perfect mixing scenarios, compared to 26% in the zero-order approximation.

soil moisture saturation. As the $\xi - s$ relation shifts to the left over time, the soil moisture threshold at which the linear approximation underestimates ξ decreases.

These results stress the importance of considering particle sizes and how they dynamically interact with the pore structure, a process that is captured by ξ and not by the common zero-order and linear approximations (Figures 5 and 6). With the same initial particle size distribution, the degree and evolution of mixing strongly modulate the extent of RP dissolution. For example, under low mixing conditions ($\alpha = 0.5$), weathering fluxes are markedly reduced compared to the perfect mixing scenario ($\alpha = 1$), with average weathering rates nearly two orders of magnitude lower and roughly three times more residual rock mass remaining after 1 year. These findings underscore the importance of mechanistic constraints imposed by soil pore structure and mixing dynamics, offering a potential explanation for the persistent gaps between predicted and observed EW fluxes in soils (Brantley, 2025; Buckingham et al., 2022; Calabrese et al., 2022; Power et al., 2025).

4. Discussion and Conclusions

Incorporating small-scale information on soil pore structure, RP characteristics, and the degree of mixing, we developed a nonlinear scaling framework to estimate the fraction of RP SA that is wet and therefore potentially

10.1029/2025WR041479

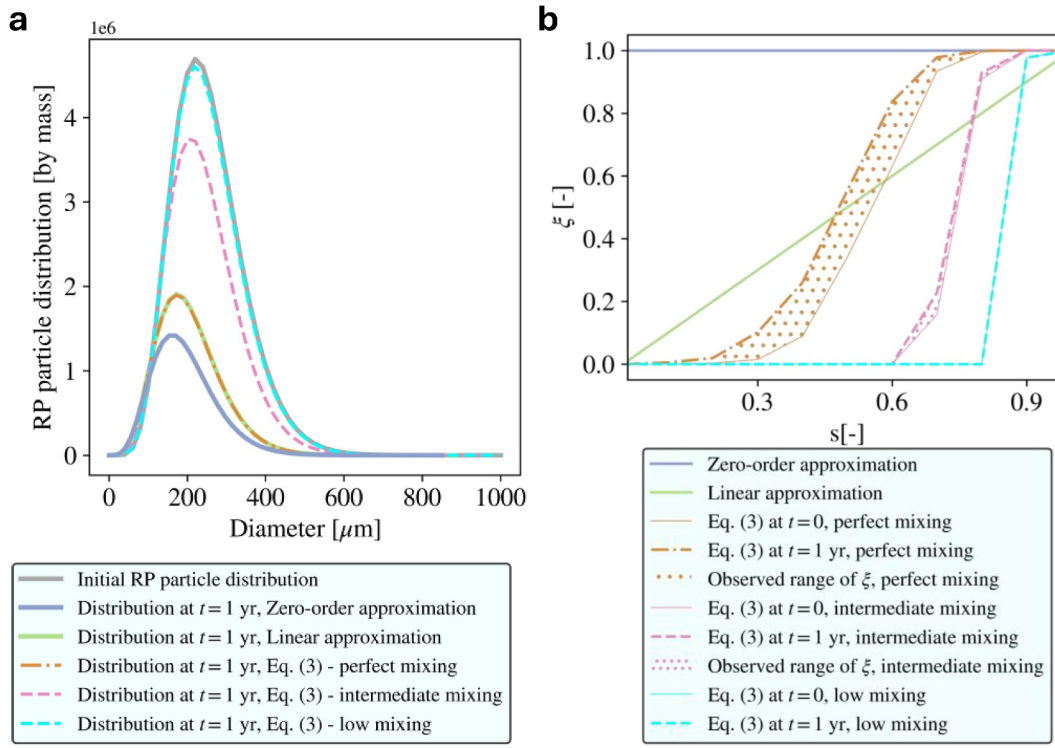

Figure 6. Evolution of the RP particle distribution under different water-rock contact scenarios considered in Figure 5. (a) The gray curve presents the initial distribution, with five colored curves showing the RP particle distribution at the end of 1 year under different $SA_{wet}(t)$ scenario runs, including the proposed role of soil pore structure and mixing degree. While the RP distribution does not shift significantly in the case of low-to-intermediate mixing, the most optimistic enhanced weathering dissolution occurs under the zero-order approximation. (b) Evolution of $\xi - s$ relationship over the year, with cyan, pink, and orange curves representing low ($\alpha = 0.5$), intermediate ($\alpha = 0.75$), and perfect mixing ($\alpha = 1$), respectively. Solid curves denote $\xi - s$ relationship at $t = 0$ and dashed curves denote the relationship at the year for all mixing scenarios, with hatching indicating the shift of $\xi - s$ curves leftward as RP particles shrink in size and migrate into smaller soil pores, maintaining the same degree of mixing over the year. The green line shows the default linear approximation, which remains unchanged throughout the simulation, and the blue line indicates the zero-order approximation, for which $\xi = 1$ throughout the year.

reactive at a given time. Using typical soil pore structures and RP particle size distributions, we showed that the wet SA scales dynamically and nonlinearly with soil moisture, marking a clear step forward from prior assumptions of zero-order (Beerling et al., 2020; Kanzaki et al., 2022; Taylor et al., 2016) or linear dependencies (Bertagni et al., 2025; Cipolla et al., 2021b).

The scaling factor, derived by linking RP SA wetness to soil pore and RP particle size distributions, suggests that the wet SA, and therefore weathering fluxes, can be substantially lower than classical EW assessments assumed in soils. For instance, the simulations in this study showed that, compared to a zero-order approximation of the wet SA, average weathering rates were reduced by approximately 14% to as much as 97%, depending on the degree of mixing, from perfect to low-mixing scenarios. While other abiotic and biotic factors undoubtedly contribute to the discrepancy observed in EW rates in soils (Brantley, 2025; Calabrese et al., 2022), our findings highlight the critical role of soil structure and particle mixing in regulating water accessibility for EW reactions, underscoring an important yet often overlooked source of uncertainty in EW assessments. This is primarily because a portion of the introduced RP particles may not come into contact with water-filled pores, either due to their coarser size or low mixing degree. As a result, there is a sharp, nonlinear reduction in dissolution rates under intermediate to dry soil moisture conditions, whereas under well-watered conditions, the scaling factor is not expected to play an important role in weathering dynamics.

Beyond the application to SMEW shown here, the scaling factor ξ can be seamlessly integrated into other continuum-scale ecohydrological and biogeochemical models, potentially enhancing their predictive capabilities without requiring computationally expensive pore-scale transport modeling (Jung & Navarre-Sitchler, 2018; L. Li

et al., 2006; Molins et al., 2012; Parmigiani et al., 2011). In vertically resolved reactive transport models (Beerling et al., 2020; K. Deng et al., 2022; Kanzaki et al., 2022; Kanzaki et al., 2024; Taylor et al., 2016), the mixing factor ξ can be assigned to each soil layer, with a clear dependence on soil depth. This allows surficial application to be represented by applying the RP only in the uppermost layers, while subsequent redistribution through rainfall, bioturbation, or tillage determines how particles move downward and become distributed within the soil pore structure. In this way, the modeling approach can potentially capture the vertical structure of RP placement under different application and mixing scenarios.

The general form of ξ in Equation 3 requires knowledge of the soil pore structure at a given time to determine the largest water-filled pore size for a given soil moisture value. In the theoretical analysis and numerical simulations presented in Section 3, we used a single soil pore size distribution ($f_p(\zeta)$) across RP mixing scenarios. This choice reflects our focus on small changes in soil properties to assess the sensitivity of simulated weathering fluxes to mixing degree under otherwise identical conditions, consistent with the simulation setup (Figure S1 in Supporting Information S1). This assumption can be relaxed for applications in which RP addition or soil disturbance processes substantially alter the pore structure. For example, as summarized in Table S1 in Supporting Information S1, we synthesized mesocosm and field EW studies to estimate changes in bulk porosity associated with different application rates, minerals, and soil types, thereby approximating the fraction of original soil pore volume occupied by rock-powder particles. Bulk soil porosity changes before and after RP application range from approximately 1%–5% Dietzen et al. (2018); Kelland et al. (2020) to as high as 12%–13% te Pas et al. (2023), the latter reflecting intentionally high application rates designed to obtain detectable short-term responses. In such cases, an updated pore size distribution should be used for each RP application when computing ξ using Equation 3 to quantify changes in soil properties and their implications for EW dissolution dynamics.

We employed Equation 4 to quantify the degree of RP mixing within the soil matrix; however, the framework is general and can accommodate any mapping function supported by theoretical or empirical observations. Recent advances in Micro-Computed Tomography for mineralogical mapping (Roslin et al., 2023) or Micro-XRF elemental mapping (Lippold et al., 2025), as well as traditional electron or optical microscopy approaches, could shed light on the distribution of the material within the soil pore space. Empirical data on mixing, although challenging to obtain, might be particularly valuable, since even small particles may cluster in large pores due to incomplete mixing, especially early in deployment before rainfall or bioturbation distributes RP particles more uniformly. This may help explain counterintuitive observations, such as finer particles dissolving more slowly than coarser ones (Amann et al., 2020), potentially due to their placement in less hydrated pores. Moreover, as RP particles dissolve, their sizes are expected to evolve, leading to a dynamic interplay between soil pore architecture and particle distribution. Smaller particles may migrate into finer pores, particularly during rainfall or irrigation events in natural or mesocosm experiments, where colloidal transport can be triggered (Calabrese et al., 2018; S. Li et al., 2013; Mohanty et al., 2015; Wang et al., 2020). The framework developed here can thus guide hypothesis testing on the roles of soil structure, particle size, and mixing degree, as well as support exploration of best-to-worst-case outcomes in EW assessments.

Correctly representing the reactive RP SA in the soil is critical for assessing the actual weathering rates, and here, we provided a mechanistic representation of it based on soil hydrology and the distributions of soil pores and RP particles. While this framework improves upon classical (zero-order) kinetic formulations (Palandri and Kharaka, 2004) for the soil environment, it does not account for other biogeochemical processes that can influence weathering fluxes, either enhancing weathering rates (e.g., biotic activity) or inhibiting them (e.g., RP particle coating). As RP dissolves and releases weathering products, concentration gradients, diffusive limitations, and local saturation conditions can arise (Andrews & Taylor, 2019; Calabrese et al., 2022; White & Brantley, 2003), especially within small-scale pores. These dynamics underscore the need for further analysis to bridge soil structure and hydrology with moisture biogeochemistry. In this direction, it would also be useful to explore how the RP addition, especially at high loads, might influence soil hydraulic properties, such as the soil water retention curve, which in turn impacts soil hydrological partitioning, vegetation growth, and the soil biota at broad.

The lack of quantitative and mechanistic parameterizations for these nano-to-microscale processes, which hinder our predictive power for EW applications and CO_2 removal potential, stems from the complexity and heterogeneity of the soil environment. Addressing this challenge requires new theoretical formulations and experimental approaches to isolate the impacts of different biogeochemical processes on weathering rates. In this context, the framework provided herein may serve as a valuable tool for investigating pore-dependent processes,

like the biotic-driven weathering that is most likely to occur at the micropore interface when moisture conditions are more hospitable for microbial growth. While the present work clarifies one key aspect of how soil structure influences EW rates, further theoretical and observational research is essential to generalize dissolution behavior across diverse soils and climates.

Conflict of Interest

The authors declare no conflicts of interest relevant to this study.

Data Availability Statement

The Python code developed for integrating the proposed scaling factor into the SMEW is available on GitHub https://github.com/ShashankAnand1996/SMEW_SS and archived on Zenodo with the doi https://doi.org/10.5281/zenodo.15749856 (Anand, 2025).

Acknowledgments
The authors acknowledge funding from the Foundation for Food and Agriculture Research, United States (22–000070), and the USDA National Institute of Food and Agriculture (Hatch project 7010390). Any opinions, findings, and conclusions or recommendations expressed in this material are those of the author(s) alone. Portions of this research were conducted with the advanced computing resources provided by Texas A&M High Performance Research Computing. Valuable remarks from the anonymous reviewers are gratefully acknowledged.

References

Abramowitz, M., & Stegun, I. A. (1965). *Handbook of mathematical functions: With formulas, graphs, and mathematical tables* (Vol. 55). Courier Corporation.

Amann, T., Hartmann, J., Struyf, E., de Oliveira Garcia, W., Fischer, E. K., Janssens, I., et al. (2020). Enhanced weathering and related element Fluxes–a cropland mesocosm approach. *Biogeosciences*, *17*(1), 103–119. https://doi.org/10.5194/bg-17-103-2020

Anand, S. K. (2025). Shashankanand1996/smew_ss: V0.1 [software]. *Zenodo*. https://doi.org/10.5281/zenodo.15749856

Andrews, M. G., & Taylor, L. L. (2019). Combating climate change through enhanced weathering of agricultural soils. *Elements: An International Magazine of Mineralogy, Geochemistry, and Petrology*, *15*(4), 253–258. https://doi.org/10.2138/gselements.15.4.253

Archer, D., Kheshgi, H., & Maier-Reimer, E. (1997). Multiple timescales for neutralization of fossil fuel co2. *Geophysical Research Letters*, *24*(4), 405–408. https://doi.org/10.1029/97gl00168

Beerling, D. J., Kantzas, E. P., Lomas, M. R., Taylor, L. L., Zhang, S., Kanzaki, Y., et al. (2025). Transforming us agriculture for carbon removal with enhanced weathering. *Nature*, *1–10*.

Beerling, D. J., Kantzas, E. P., Lomas, M. R., Wade, P., Eufrasio, R. M., Renforth, P., et al. (2020). Potential for large-scale co2 removal via enhanced rock weathering with croplands. *Nature*, *583*(7815), 242–248. https://doi.org/10.1038/s41586-020-2448-9

Bertagni, M. B., Calabrese, S., Cipolla, G., Noto, L. V., & Porporato, A. (2025). Advancing enhanced weathering modeling in soils: Critical comparison with experimental data. *Journal of Advances in Modeling Earth Systems*, *17*(1), e2024MS004224. https://doi.org/10.1029/2024ms004224

Bertagni, M. B., & Porporato, A. (2022). The carbon-capture efficiency of natural water alkalinization: Implications for enhanced weathering. *Science of The Total Environment*, *838*, 156524. https://doi.org/10.1016/j.scitotenv.2022.156524

Brantley, S. L. (2025). Understanding the lab-field discrepancy in mineral dissolution from flasks to enhanced rock weathering. *Reviews of Geophysics*, *63*(4), e2025RG000881. https://doi.org/10.1029/2025RG000881

Brooks, R. H. (1965). *Hydraulic properties of porous media*. Colorado State University.

Brutsaert, W. (2023). *Hydrology: An introduction*. Cambridge University Press.

Buckingham, F., Henderson, G. M., Holdship, P., & Renforth, P. (2022). Soil core study indicates limited co2 removal by enhanced weathering in dry croplands in the UK. *Applied Geochemistry*, *147*, 105482. https://doi.org/10.1016/j.apgeochem.2022.105482

Calabrese, S., & Porporato, A. (2020). Wetness controls on global chemical weathering. *Environmental Research Communications*, *2*(8), 085005. https://doi.org/10.1088/2515-7620/abad7b

Calabrese, S., Richter, D. D., & Porporato, A. (2018). The formation of clay-enriched horizons by lessivage. *Geophysical Research Letters*, *45*(15), 7588–7595. https://doi.org/10.1029/2018gl078778

Calabrese, S., Wild, B., Bertagni, M. B., Bourg, I. C., White, C., Aburto, F., et al. (2022). Nano-to global-scale uncertainties in terrestrial enhanced weathering. In *Environmental Science & Technology*. (Publisher: American Chemical Society). https://doi.org/10.1021/acs.est.2c03163

Cipolla, G., Calabrese, S., Noto, L. V., & Porporato, A. (2021a). The role of hydrology on enhanced weathering for carbon sequestration ii. From hydroclimatic scenarios to carbon-sequestration efficiencies. *Advances in Water Resources*, *154*, 103949. https://doi.org/10.1016/j.advwatres.2021.103949

Cipolla, G., Calabrese, S., Noto, L. V., & Porporato, A. (2021b). The role of hydrology on enhanced weathering for carbon sequestration i. Modeling rock-dissolution reactions coupled to plant, soil moisture, and carbon dynamics. *Advances in Water Resources*, *154*, 103934. https://doi.org/10.1016/j.advwatres.2021.103934

Clarkson, M. O., Larkin, C. S., Swoboda, P., Reershemius, T., Suhrhoff, T. J., Maesano, C. N., & Campbell, J. S. (2024). A review of measurement for quantification of carbon dioxide removal by enhanced weathering in soil. *Frontiers in Climate*, *6*, 1345224. https://doi.org/10.3389/fclim.2024.1345224

Deng, H., Sonnenthal, E., Arora, B., Breunig, H., Brodie, E., Kleber, M., et al. (2023). The environmental controls on efficiency of enhanced rock weathering in soils. *Scientific Reports*, *13*(1), 9765. https://doi.org/10.1038/s41598-023-36113-4

Deng, K., Yang, S., & Guo, Y. (2022). A global temperature control of silicate weathering intensity. *Nature Communications*, *13*(1), 1781. https://doi.org/10.1038/s41467-022-29415-0

Dexter, A., Czyż, E., Richard, G., & Reszkowska, A. (2008). A user-friendly water retention function that takes account of the textural and structural pore spaces in soil. *Geoderma*, *143*(3–4), 243–253. https://doi.org/10.1016/j.geoderma.2007.11.010

Dietzen, C., Harrison, R., & Michelsen-Correa, S. (2018). Effectiveness of enhanced mineral weathering as a carbon sequestration tool and alternative to agricultural lime: An incubation experiment. *International Journal of Greenhouse Gas Control*, *74*, 251–258. https://doi.org/10.1016/j.ijggc.2018.05.007

Ding, D., Zhao, Y., Feng, H., Peng, X., & Si, B. (2016). Using the double-exponential water retention equation to determine how soil pore-size distribution is linked to soil texture. *Soil and Tillage Research*, *156*, 119–130. https://doi.org/10.1016/j.still.2015.10.007

Dlapa, P., Hrinik, D., Hrabovskỳ, A., Šimkovic, I., Žarnovičan, H., Sekucia, F., & Kollar, J. (2020). The impact of land-use on the hierarchical pore size distribution and water retention properties in loamy soils. *Water*, *12*(2), 339. https://doi.org/10.3390/w12020339

Gaucher, Y., Tanaka, K., Johansson, D. J., Goll, D. S., & Ciais, P. (2025). Leveraging ecosystems responses to enhanced rock weathering in mitigation scenarios. *Nature Communications*, *16*(1), 3021. https://doi.org/10.1038/s41467-025-58284-6

Hartmann, J., West, A. J., Renforth, P., Köhler, P., De La Rocha, C. L., Wolf-Gladrow, D. A., et al. (2013). Enhanced chemical weathering as a geoengineering strategy to reduce atmospheric carbon dioxide, supply nutrients, and mitigate ocean acidification. *Reviews of Geophysics*, *51*(2), 113–149. https://doi.org/10.1002/rog.20004

Hill, R., Horton, R., & Cruse, R. (1985). Tillage effects on soil water retention and pore size distribution of two mollisols. *Soil Science Society of America Journal*, *49*(5), 1264–1270. https://doi.org/10.2136/sssaj1985.03615995004900050039x

Hillel, D. (2013). *Fundamentals of soil physics*. Academic Press.

Hunt, A. (2021). Soil formation, vegetation growth, and water balance: A theory for budyko. *Hydrogeology, chemical weathering, and soil formation*, 67–80.

Jung, H., & Navarre-Sitchler, A. (2018). Physical heterogeneity control on effective mineral dissolution rates. *Geochimica et Cosmochimica Acta*, *227*, 246–263. https://doi.org/10.1016/j.gca.2018.02.028

Kantzas, E. P., Val Martin, M., Lomas, M. R., Eufrasio, R. M., Renforth, P., Lewis, A. L., et al. (2022). Substantial carbon drawdown potential from enhanced rock weathering in the United Kingdom. *Nature Geoscience*, *15*(5), 382–389. https://doi.org/10.1038/s41561-022-00925-2

Kanzaki, Y., Chiaravalloti, I., Zhang, S., Planavsky, N. J., & Reinhard, C. T. (2024). In silico calculation of soil ph by scepter v1. 0. *Geoscientific Model Development*, *17*(10), 4515–4532. https://doi.org/10.5194/gmd-17-4515-2024

Kanzaki, Y., Zhang, S., Planavsky, N. J., & Reinhard, C. T. (2022). Soil cycles of elements simulator for predicting terrestrial regulation of greenhouse gases: Scepter v0. 9. *Geoscientific Model Development*, *15*(12), 4959–4990. https://doi.org/10.5194/gmd-15-4959-2022

Kelland, M. E., Wade, P. W., Lewis, A. L., Taylor, L. L., Sarkar, B., Andrews, M. G., et al. (2020). Increased yield and co2 sequestration potential with the c4 cereal sorghum bicolor cultivated in basaltic rock dust-amended agricultural soil. *Global Change Biology*, *26*(6), 3658–3676. https://doi.org/10.1111/gcb.15089

Klemme, A., Rixen, T., Müller, M., Notholt, J., & Warneke, T. (2022). Destabilization of carbon in tropical peatlands by enhanced weathering. *Communications Earth and Environment*, *3*(1), 212. https://doi.org/10.1038/s43247-022-00544-0

Köhler, P., Hartmann, J., & Wolf-Gladrow, D. A. (2010). Geoengineering potential of artificially enhanced silicate weathering of olivine. *Proceedings of the National Academy of Sciences*, *107*(47), 20228–20233.

Laio, F., Porporato, A., Ridolfi, L., & Rodriguez-Iturbe, I. (2001). Plants in water-controlled ecosystems: Active role in hydrologic processes and response to water stress: Ii. Probabilistic soil moisture dynamics. *Advances in Water Resources*, *24*(7), 707–723. https://doi.org/10.1016/s0309-1708(01)00005-7

Li, L., Peters, C. A., & Celia, M. A. (2006). Upscaling geochemical reaction rates using pore-scale network modeling. *Advances in Water Resources*, *29*(9), 1351–1370. https://doi.org/10.1016/j.advwatres.2005.10.011

Li, S., Li, H., Xu, C.-Y., Huang, X.-R., Xie, D.-T., & Ni, J.-P. (2013). Particle interaction forces induce soil particle transport during rainfall. *Soil Science Society of America Journal*, *77*(5), 1563–1571. https://doi.org/10.2136/sssaj2013.01.0009

Li, X., & Zhang, L. (2009). Characterization of dual-structure pore-size distribution of soil. *Canadian Geotechnical Journal*, *46*(2), 129–141. https://doi.org/10.1139/t08-110

Lippold, E., Landl, M., Braatz, E., Schlüter, S., Kilian, R., Mikutta, R., et al. (2025). Linking micro-x-ray fluorescence spectroscopy and x-ray computed tomography with model simulation explains differences in nutrient gradients around roots of different types and ages. *New Phytologist*, *246*(4), 1780–1795. https://doi.org/10.1111/nph.70102

Michaelowa, A., Honegger, M., Poralla, M., Winkler, M., Dalfiume, S., & Nayak, A. (2023). International carbon markets for carbon dioxide removal. *PLOS Climate*, *2*(5), e0000118. https://doi.org/10.1371/journal.pclm.0000118

Mohanty, S. K., Saiers, J. E., & Ryan, J. N. (2015). Colloid mobilization in a fractured soil during dry–wet cycles: Role of drying duration and flow path permeability. *Environmental science & technology*, *49*(15), 9100–9106. https://doi.org/10.1021/acs.est.5b00889

Molins, S., Trebotich, D., Steefel, C. I., & Shen, C. (2012). An investigation of the effect of pore scale flow on average geochemical reaction rates using direct numerical simulation. *Water Resources Research*, *48*(3), W03527. https://doi.org/10.1029/2011wr011404

Mualem, Y. (1976). A new model for predicting the hydraulic conductivity of unsaturated porous media. *Water Resources Research*, *12*(3), 513–522. https://doi.org/10.1029/wr012i003p00513

Nimmo, J. R. (2004). Porosity and pore size distribution. *Encyclopedia of Soils in the Environment*, *3*(1), 295–303.

Pačes, T. (1983). Rate constants of dissolution derived from the measurements of mass balance in hydrological catchments. *Geochimica et Cosmochimica Acta*, *47*(11), 1855–1863. https://doi.org/10.1016/0016-7037(83)90202-8

Palandri, J. L., & Kharaka, Y. K. (2004). A compilation of rate parameters of water-mineral interaction kinetics for application to geochemical modeling.

Parmigiani, A., Huber, C., Bachmann, O., & Chopard, B. (2011). Pore-scale mass and reactant transport in multiphase porous media flows. *Journal of Fluid Mechanics*, *686*, 40–76. https://doi.org/10.1017/jfm.2011.268

Paulo, C., Power, I. M., Stubbs, A. R., Wang, B., Zeyen, N., & Wilson, S. (2021). Evaluating feedstocks for carbon dioxide removal by enhanced rock weathering and co2 mineralization. *Applied Geochemistry*, *129*, 104955. https://doi.org/10.1016/j.apgeochem.2021.104955

Porporato, A., & Yin, J. (2022). *Ecohydrology: Dynamics of life and water in the critical zone*. Cambridge University Press.

Power, I. M., Hatten, V. N., Guo, M., Schaffer, Z. R., Rausis, K., & Klyn-Hesselink, H. (2025). Are enhanced rock weathering rates overestimated? A few geochemical and mineralogical pitfalls. *Frontiers in Climate*, *6*, 1510747. https://doi.org/10.3389/fclim.2024.1510747

Renforth, P., & Campbell, J. S. (2021). The role of soils in the regulation of ocean acidification. *Philosophical Transactions of the Royal Society B*, *376*(1834), 20200174. https://doi.org/10.1098/rstb.2020.0174

Renforth, P., & Henderson, G. (2017). Assessing ocean alkalinity for carbon sequestration. *Reviews of Geophysics*, *55*(3), 636–674. https://doi.org/10.1002/2016RG000533

Roslin, A., Marsh, M., Provencher, B., Mitchell, T., Onederra, I., & Leonardi, C. (2023). Processing of micro-ct images of granodiorite rock samples using convolutional neural networks (cnn), part ii: Semantic segmentation using a 2.5d cnn. *Minerals Engineering*, *195*, 108027. https://doi.org/10.1016/j.mineng.2023.108027

Smith, S., Geden, O., Gidden, M., Lamb, W., Nemet, G., Minx, J., et al. (2024). The state of carbon dioxide removal.

Sovacool, B. K., Baum, C. M., & Low, S. (2023). Reviewing the sociotechnical dynamics of carbon removal. *Joule*, *7*(1), 57–82. https://doi.org/10.1016/j.joule.2022.11.008

Strefler, J., Amann, T., Bauer, N., Kriegler, E., & Hartmann, J. (2018). Potential and costs of carbon dioxide removal by enhanced weathering of rocks. *Environmental Research Letters*, *13*(3), 034010. https://doi.org/10.1088/1748-9326/aaa9c4

Sverdrup, H., & Warfvinge, P. (1988). Weathering of primary silicate minerals in the natural soil environment in relation to a chemical weathering model. *Water, Air, and Soil Pollution*, *38*(3–4), 387–408. https://doi.org/10.1007/bf00280768

Taylor, L. L., Quirk, J., Thorley, R., Kharecha, P. A., Hansen, J., Ridgwell, A., et al. (2016). Enhanced weathering strategies for stabilizing climate and averting ocean acidification. *Nature Climate Change*, *6*(4), 402–406. https://doi.org/10.1038/nclimate2882

te Pas, E. E., Hagens, M., & Comans, R. N. (2023). Assessment of the enhanced weathering potential of different silicate minerals to improve soil quality and sequester co2. *Frontiers in Climate*, *4*, 954064. https://doi.org/10.3389/fclim.2022.954064

Van Genuchten, M. T. (1980). A closed-form equation for predicting the hydraulic conductivity of unsaturated soils. *Soil Science Society of America Journal*, *44*(5), 892–898. https://doi.org/10.2136/sssaj1980.03615995004400050002x

Wang, C., Wang, R., Huo, Z., Xie, E., & Dahlke, H. E. (2020). Colloid transport through soil and other porous media under transient flow conditions—a review. *Wiley Interdisciplinary Reviews. Water*, *7*(4), e1439. https://doi.org/10.1002/wat2.1439

White, A. F., & Blum, A. E. (1995). Effects of climate on chemical_weathering in watersheds. *Geochimica et Cosmochimica Acta*, *59*(9), 1729–1747. https://doi.org/10.1016/0016-7037(95)00078-e

White, A. F., & Brantley, S. L. (2003). The effect of time on the weathering of silicate minerals: Why do weathering rates differ in the laboratory and field? *Chemical Geology*, *202*(3–4), 479–506. https://doi.org/10.1016/j.chemgeo.2003.03.001

White, A. F., & Brantley, S. L. (2018). *Chemical weathering rates of silicate minerals* (Vol. 31). Walter de Gruyter GmbH and Co KG.

Wildenschild, D., & Sheppard, A. P. (2013). X-ray imaging and analysis techniques for quantifying pore-scale structure and processes in subsurface porous medium systems. *Advances in Water Resources*, *51*, 217–246. https://doi.org/10.1016/j.advwatres.2012.07.018

Zhang, S., Reinhard, C. T., Liu, S., Kanzaki, Y., & Planavsky, N. J. (2025). A framework for modeling carbon loss from rivers following terrestrial enhanced weathering. *Environmental Research Letters*.